

www.acsami.org Research Article

Polymer N-Heterocyclic Carbene (NHC) Ligands for Silver Nanoparticles

girchare իկի es լի ayreetive Muleaj, Aleisha Price, Kecheng Wei, Qiang Luo, Srinivas Thanneeru,



Cite This: *ACS Appl. Mater. Interfaces* 2022, 14, 55227–55237



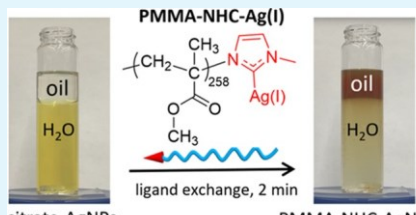
ACCES\$

Metrics & More

Article Recommendations

Supporting Information

ABSTRACT. Polymer *N*-heterocyclic carbenes (NHCs) are a class of robust surface ligands to provide superior colloidal stability for metal nanoparticles (NPs) under various harsh conditions. We report a general method to prepare polymeric NHCs and demonstrate that these polymer NHC-AgNPs are stable against oxidative etching and show high peroxidase activity. We prepared three imidazolium-terminated poly(methyl methacrylate) (PMMA), polystyrene (PS), and poly(2-(2-methoxyethoxy)ethyl methacrylate) (PMEO₂MA) through atom-transfer radical polymerization with an imidazole-containing initiator. The imidazolium end group was further converted to NHC-Ag(I) in the presence of Ag₂O at room temperature. Polymer NHC-Ag(I) can



citrate-AgNPs

PMMA-NHC-AgNPs

transmetalate to AgNPs through ligand exchange at the interface of oil/water within 2 min. All the three polymers can modify metal NPs, such as AgNPs, Ag nanowires, and AuNPs, providing excellent thermal, oxidative, and chemical stabilities for AgNPs. As an example, in the presence of hydrogen peroxide, AgNPs modified by polymer NHCs were resistant against oxidative etching with a rate of \sim 700 times slower than those grafted with thiolates. AgNPs modified by polymer NHCs also showed higher peroxidase activity, 4 times more active than those capped by citrate and polyvinylpyrrolidone (PVP) and 2 times more active than those with polymer thiolate. Our studies demonstrate a great potential of using polymer NHCs to stabilize metallic NPs for various applications.

KEYWORDS: polymer N-heterocyclic carbenes, metal nanoparticles, transmetalation, ligand exchange, colloidal stability, peroxidase activity

1. INTRODUCTION

Polymer-grafted plasmonic nanoparticles (PGNPs) consist of core metal NPs grafted by a layer of well-defined polymer tethers. As hybrids, plasmonic NPs provide interesting optical properties, for example, localized surface plasmon resonance (LSPR), while polymer tethers form a dense organic shell that improves colloidal stability and enables the versatile surface functionalization of NP cores. Therefore, PGNPs have been demonstrated for a broad range of applications in nanomedicine¹⁻⁵ and catalysis.⁶⁻¹³ Polymer ligands usually rely on the binding motif covalently tagged on polymers to bind with metal NPs through coordination interaction. 13-15 Thiol has been a popular binding motif due to its strong binding power to metals and its ease of synthesis via reversible addition fragmentation chain transfer (RAFT) polymerization. However, metal thiolate binding is unstable under redox conditions or at elevated temperatures. 20,21 Therefore, polymer thiolate-bound metal NPs are often subject to thermal and oxidation degradation.

N-Heterocyclic carbenes (NHCs) attract tremendous interest as a strong binding motif to modify metal NPs. NHCs contain a neutral carbon with a pair of electrons on the nitrogen-containing heterocyclic ring. The σ donation makes the NHCs bind with a number of metal atoms through metal—carbon interaction. NHCs have a high bonding energy with

various transition metals, for example, 158 kJ/mol for NHC-Au,7,41,42 that is stronger than that of other ligands, such as thiolate and phosphine with bonding energies of 126 and 137 kJ/mol, 43 respectively. The metal-carbon bond is stable under harsh conditions, for example, thermal annealing and redox. Early examples from Fairlamb and Checkhik show that NHCs can modify oil-phase noble metal NPs via ligand exchange. However, free NHCs require anhydrous and non-aerobic conditions, which limit their applications for metal NPs prepared in an aqueous solution. 45 On the other hand, NHCs can "graft to" metal NPs through ligand exchange with NHCmetal complexes or imidazolium. 30,46 A few reported examples recently demonstrated the "grafting-to" method of polymeric NHCs to prepare PGNPs with metal NPs in water. 6,7,47 Starting with halogen-ended polymers synthesized via atomtransfer radical polymerization (ATRP), we have demonstrated the versatile synthesis of NHC-Cu(I) or imidazoliumterminated polymers, as NHC precursors, through end group

Received: September 30, 2022 Accepted: November 18, 2022 Published: December 2, 2022





© 2022 American Chemical Society

https://doi.org/10.1021/acsami.2c17706

Scheme 1. (a) Synthesis of PMMA-IM and PMMA-NHC-Ag(I). (b-d) Chemical Structures of (b) PS-NHC-Ag(I), (c) PMEO₂MA-NHC-Ag(I), and (d) PS-SH

Table 1. Synthesis and Characterization of Imidazolium and NHC-Ag(I)-Ended Polymers

sample		molecular weight (kg/mol)		
	composition	$M_{n,NMR}$	$M_{n,GPC}$	dispersity (Θ) (M_w/M_n)
P1	PMMA ₂₅₈ -IM	26.1	30.0	1.2
P1-NHC	PMMA ₂₅₈ -NHC-Ag(I)		31.2	1.2
P2	PMEO ₂ MA ₁₄₅ -IM	27.3	32.4	1.2
P2-NHC	PMEO ₂ MA ₁₄₅ -NHC-Ag(I)		33.6	1.2
P3	PS ₁₂₀ -IM	12.7	11.1	1.2
P3-NHC	PS_{120} -NHC-Ag(I)		11.2	1.2
P4	PS ₁₃₄ -SH	14.2	17.7	1.1

functionalization. Either NHC-Cu(I) or imidazolium-termimaterias lymerae were able to waved if you within In this paper, we report a facile method to use polymer-NHC-Ag(I) complex as a transmetalation agent to functionalize metal NPs synthesized in aqueous solutions. NHC-Ag(I) arean rideal transmetalatien agant leas been opravious la diagrama de la composición a relatively small bonding energy as compared to other NHCtransition ratals complexes during the Averaker an bassind opination

Ag(I) to transmetalate with another metal. We first synthesized polymer-NHC-Ag(I) through imidazolium-ended polymers prepared via ATRP. Three NHC-Ag(I)-terminated polymers were prepared, namely, poly(methyl methacrylate) (PMMA), polystyrene (PS), and poly(2-(2-methoxyethoxy)ethyl methacrylate) (PMEO₂MA) (Scheme 1). These three polymers could modify metal NPs, such as AgNPs, Ag nanowires, and AuNPs, at the interface of oil/water. To show the robustness of polymer NHCs on the surface of metal NPs, we compared the stability of polymer NHC-grafted AgNPs with polymer thiolate and citrate under oxidative, chemical, and thermal annealing conditions. We showed that PS₁₂₀-NHC could slow down the dissolution rate of AgNPs by approximately 700-fold as chimatedowith the areating sava Envithed at pinythe presence grafted AgNPs were examined using the oxidation of 4meoxylphenol (4-MEOP) as a model reaction. AgNPs modified by PS₁₂₀-NHCs were about 4 times more reactive than those capped with citrate and polyvinylpyrrolidone (PVP)

and 2 times more reactive than those with PS₁₃₄-SH. Our ligand-exchange method provides a general strategy to stabilize metal NPs with polymer NHCs under various harsh conditions.

2. RESULTS AND DISCUSSION

Polymer NHC ligands were synthesized via ATRP as shown in Scheme 1. An imidazole-containing ATRP initiator (IM-Br) was prepared through the coupling reaction of 1-(2hydroxyethyl)imidazole (IM-OH) and 2-bromo-2-methylpropionyl bromide (BMPB).⁴⁷ Using IM-Br as the ATRP initiator, imidazole-ended polymers, for example, methyl methacrylate (MMA) used to prepare the imidazole-ended homopolymer of PMMA, were further synthesized (Scheme 1). The synthetic details are given in the Experimental Section (see characterization in Figures S1-S2). The methylation of imidazole as a post-polymerization functionalization was carried out by mixing imidazole-ended PMMA and iodomethane (CH3I) in dichloromethane (DCM) at room temperature overnight to yield imidazolium-terminated PMMA (denoted as PMMA-IM or P1, Table 1). The number-average molecular weight (M_n) and dispersity (Đ) of PMMA measured by gel permission chromatography (GPC) calibrated with polystyrene (PS) are 30.0 kg/mol and 1.2, respectively. From ¹H NMR, the number of repeat units of PMMA determined using the proton peak of imidazole (N-CH-N) at 9.6 ppm as the integration standard is 258. The conversion of imidazolium to NHC-Ag(I) was SAFFIAND FOND PINNING PANAMA-AND (WINDER-ASIDED IN HEROLOGY CAPIK NMR where the proton peak of -N-CH-N- on the imidazole

since the Gonpmedisapprediction that stello stitution have (1). Ag(I), the dimers of NHC-Ag-NHC were not seen in PMMA-NHC-Ag(I) as confirmed by GPC (Table 1), different from the molecular NHC-Ag(I) species. 49 Using a similar method, PMEO₂MA-NHC-Ag(I) (P2) and PS-NHC-Ag(I) (P3) were prepared, and their characterization details are summarized in Figures S3-S6. As a control, we also prepared thiol-terminated PS (PS₁₃₄-SH, P4) using *n*-butyl action for reduce that to this easier teans as you that it and by the property by timestration and production and the contraction of PS are 17.7 kg/mol and 1.1, respectively.

The surface modification of AgNPs was carried out using a biphasic ligand-exchange method. Citrate-capped AgNPs (average diameter of 27 nm) were prepared by reducing AgNO₃ with sodium citrate and ascorbic acid according to the previous literature with the minor modification. 52,53 Typically, the ligand exchange was carried out at the interface of water and toluene. In a 20 mL vial, 10 mL of the AgNP aqueous solution (0.05 mg/mL) was added, followed by another 5 mL of PMMA-NHC-Ag(I) dissolved in toluene at a concentration of 0.4 mg mL⁻¹. The solution mixture had a clear interface where the top polymer solution was colorless and the bottom layer containing AgNPs was pale-yellow. After the solution was further stirred vigorously for 2 min, the phase transfer of AgNPs from water to toluene was observed, as evidenced by transferring the yellowish color to the top layer, while the aqueous bottom layer became colorless. The toluene phase was then collected, and polymer-grafted AgNPs (PMMA-NHC-AgNPs) were centrifuged in toluene four times to remove the free polymers. PMMA-NHC as a strong binding motif can bind with AgNPs through trans-metalation. The modification is facile and rapid, similar to our previous reports with AuNPs and polymeric NHC-Cu(I). 7,47 Figure 1c shows the UV-vis spectra of citrate-capped AgNPs and PMMA-NHC-AgNPs. The LSPR of citrate-capped AgNPs is at 408 nm. After surface modification, PMMA-NHC-AgNPs

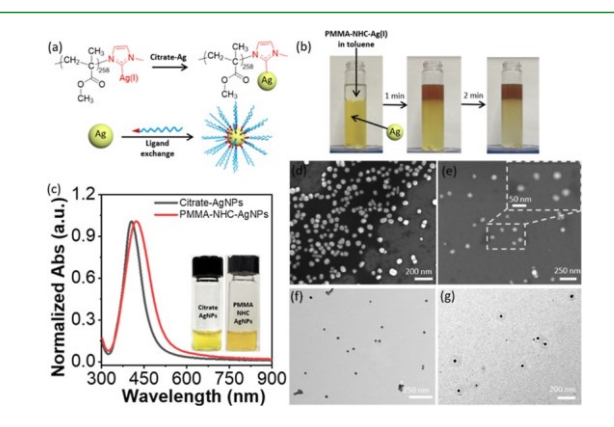


Figure 1. (a) Chemical structure of PMMA and scheme showing the NHC-Ag(I)-terminated PMMA to modify AgNPs via ligand PRYSIDENSIFON 65 HAZISBEEP INTO MAIN THOSE PARTIES ON LIGHT (CEXCHARD SIGN LIGHT) inclosure resolution lawer) and 10 control siteater cannow has the control of the citrate-capped AgNPs and PMMA-NHC-modified AgNPs. (d-g) Representative SEM and TEM image showing (d,f) citrate-capped AgNPs and (e,g) PMMA-NHC-AgNPs.

have a red shift of \sim 12 nm due to the changes in the refraction instably and the Nother bigged of and Malverth CT has notice WAREDSEON FIRSTAND AND STEIMING NAMED IN THE PROPERTY OF THE P clear polymer shell with a thickness of ~15 nm on the surface of AgNPs compared to citrate-capped AgNPs with a diameter of 27 nm (Figure 1e). The grafting density of PMMA-NHC

was calculated to be ~0.13 chains nm from SEM images. The calculation details are shown in the Supporting Information.

We examined the solubility of PMMA-NHC-AgNPs in different organic solvents. After centrifugation, PMMA-NHC-AgNPs could be dispersed in any good solvents of PMMA such as anisole, acetone, dimethyl sulfoxide (DMSO), tetrahydrofuran (THF), dichloromethane (DCM), dimethylformamide (DMF), and dimethylacetamide (DMAc). The dispersion of the PMMA-modified AgNPs has a yellow color (Figure 2). The corresponding LSPR peak of AgNPs in all

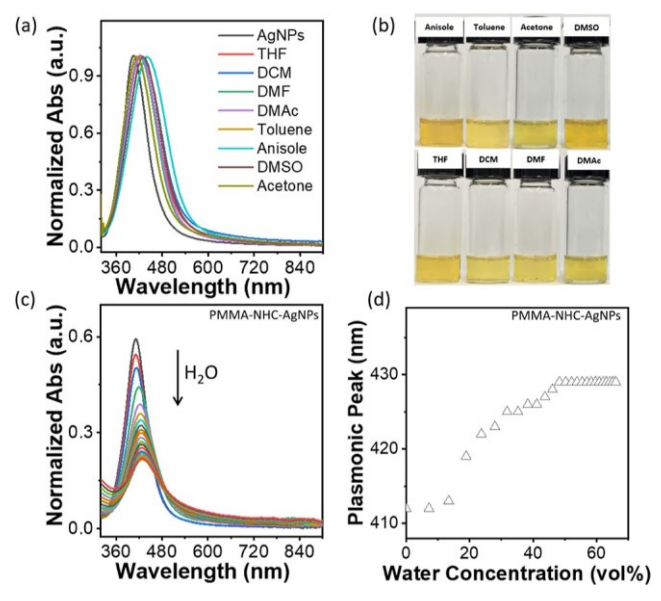


Figure 2. (a) UV-vis spectra of PMMA-NHC-AgNPs in various solvents. (b) Images showing the dispersity in different organic solvents. (c) Determination of C_{cwc} of PMMA-NHC-AgNPs using UV-vis spectroscopy. The UV-vis spectra of PMMA-NHC-AgNPs and 5 vol % per 1 min. (d) Plasmonic peak of PMMA-NHC-AgNPs as a function of the water concentration in DMF.

solvents is around 420 nm. indicating that PMMA-NHCs stabilize AgNPs in organic solvents against aggregation. The change in surface hydrophobicity of PMMA-NHC-AgNPs was also investigated through water titration.

th When mater mascoatin pusish valded to id Metalingersialing would collapse with AgNPs, leading to the aggregation of AgNPs. The titration was in situ followed using UV-vis spectroscopy (Figure 2c). The LSPR of AgNPs showed a clear red shift with the gradual increase of water concentration. By plotting the LSPR peak against water concentration, we defined the abrupt increase of the LSPR peak as the critical water concentration (C_{CWC}) (Figure 2d). The C_{CWC} of PMMA-NHC-AgNPs is 18% in DMF. This result is close to the Convis of Clark as the other arrey our World Taggred as bift We further used TEM to confirm the AgNP aggregates (Figure S7). In the mixture of water/DMF, PMMA-NHC-AgNPs by seeded agoung gregates middle by his polymore laway pould be

To further confirm the appearance of PMMA on AgNPs, ¹H NMR spectroscopy was used to examine the proton chemical shift on the NHC end group. As shown in Figure 3a, PMMA-

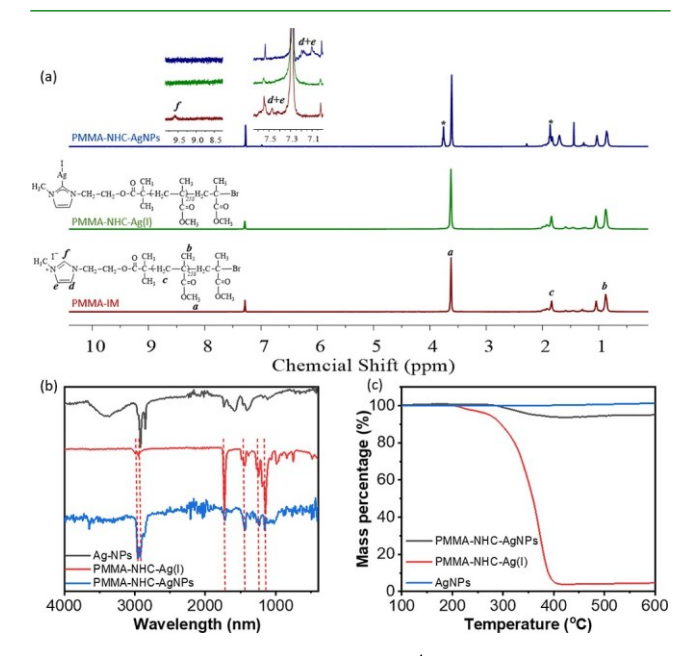


Figure 3. (a) Chemical structures and ¹H NMR spectra showing PMMA-IM, PMMA-NHC-Ag(I), and PMMA-NHC-AgNPs. * is the relivent agriph approximate with the showing the weight loss percentage of citrated acid-capped AgNPs, PMMA-NHC-Ag, and PMMA-modified AgNPs.

IM shows the typical resonance peaks of -CH₃- (peak b) at 0.8-1.1 ppm, $-CH_2$ - (peak c) at 1.8-2.1 ppm, and $-OCH_3$ - at 3.5 ppm. The vinyl protons (N-CH \diamondsuit CH-N, d + e) on the imidazolium ring appear at 7.4-7.5 ppm. The imidazolium proton (N-CH-N, f) appears at 9.6 ppm. After the reaction with Ag_2O , the replacement of the proton f by Ag(I) is clear where the proton peak disappeared. Meanwhile, the proton peaks of d + e shifted to a lower chemical shift overlap with the solvent peak of CHCl₃. After the surface modification with AgNPs, the proton f at 9.6 ppm was still absent. The transmetalation between NHC-Ag(I) and AgNPs did have an impreseton the vinn! the tennenwhite of those virtual pearenss inchisative his fis proton econicoente twith relation and of relation AgNPs where more metallic Ag atoms likely vary the electron density of bound Ag atoms as compared to individual Ag(I) in PMMA-NHC-Ag(I). The chemical shift of those vinyl protons is close to our previously reported results on NHC-AuNPs. 7,47 Furthermore, the characteristic peaks from PMMA, for example, -OCH₃- on the side chains at 3.5 ppm and proton peaks on the backbone at 1.8-2.1 ppm, are consistent with PMMA-IM and PMMA-NHC-Ag(I).

PMIMA NAGHONG (the ARD SPANNA ON THE TEACH PROPERTY OF THE PRO

the C-H asymmetric and symmetric stretching of PMMA, while PMMA-NHC-AgNPs did not have the broad peak from the O-H stretching as citrate-capped AgNPs. The two peaks at 14071 to 1579 cm⁻¹ correspond to the C&O asymmetric and symmetric stretching of the carboxylate ion, respectively. The peaks at 1260 to 1000 cm⁻¹ are representative of the C-O stretching. These peaks confirmed that PMMA plays the surface ligand to stabilize AgNPs. The grafting density of PMMA-NHC on AgNPs was estimated by thermogravimetric analysis (TGA) (Figure 3c). Using the weight loss of PMMA at 285-400 °C, the density of PMMA-NHC was estimated to be 0.08 chains nm $^{-2}.$ This is approximately close to $\sim\!131$ chains per AgNP with an average size of 27 nm. The grafting density is close to the value calculated from SEM. The calculation details are shown in the Supporting Information. As compared to PS-SH where the grafting density usually reached 0.1-0.3 chains nm⁻² in grafting to approach with modification >6 h, 7,55 the grafting density of PMMA-NHC on AgNPs is remarkable given 2 min of surface modification. The grafting density of PMMA-NHC is also close to the ligand density of polymer NHCs reported previously.7,47,56

Hydrophilic PMEO₂MA-IM (P2) and hydrophobic PS-IM (P3) can also be used as surface ligands for AgNPs. Using similar synthetic and ligand-exchange procedures, PMEO₂MA-NHC-Ag(I) can modify AgNPs in a single phase of water. PMEO₂MA-NHC-grafted AgNPs can be dispersed not only in organic solvents such as THF, DMF, and DMSO but also in water (Figure 4a). As shown in Figure S8, the hydrodynamic radius of citrate AgNPs and PMEO₂MA-NHC-AgNPs in water are 14 and 19 nm, respectively. It further confirmed that PMEO₂MA-NHC replaced citrate to graft on the surface of AgNPs. Also, PMEO₂MA-NHC-modified AgNPs can be stored in water for >11 months without aggregation as shown in Figure S9. The

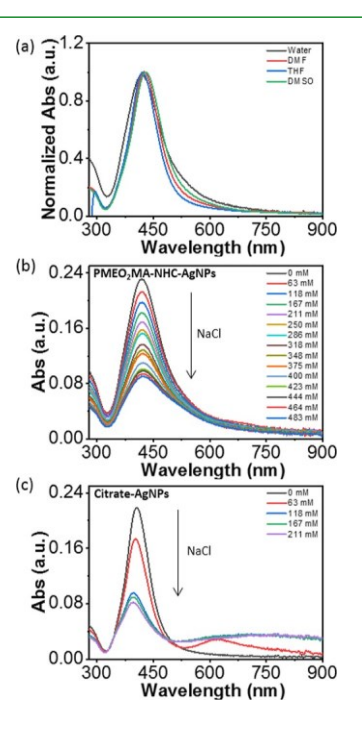
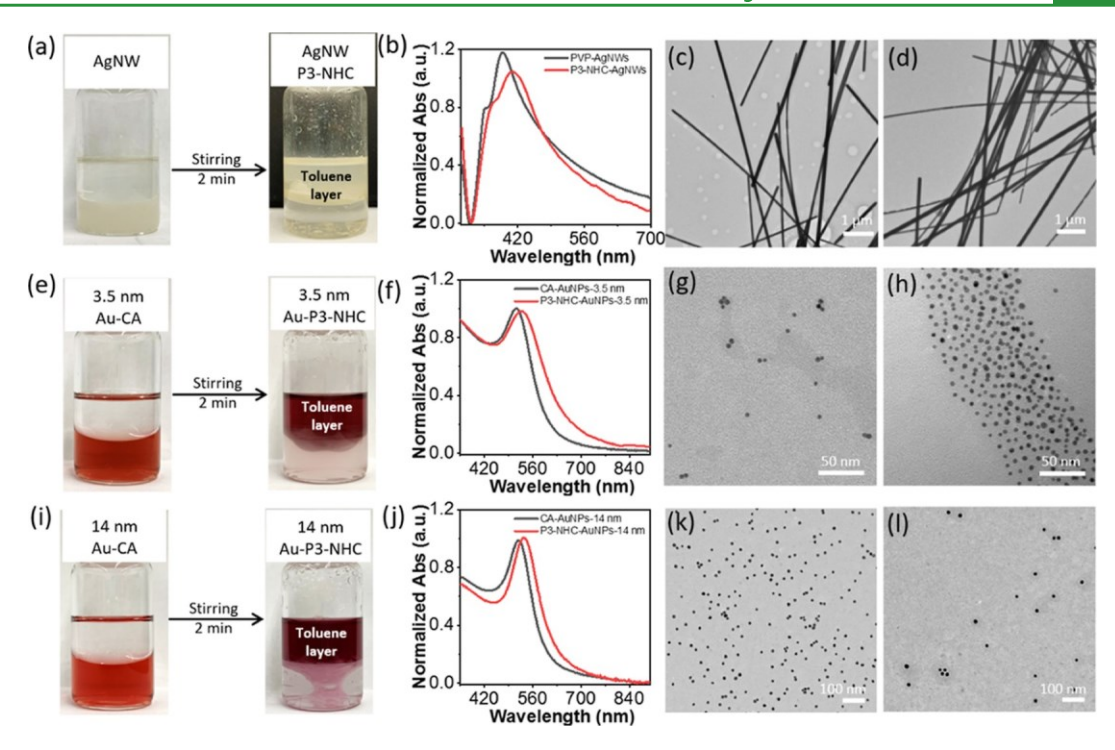


Figure 4. (a) UV-vis spectra of PMEO $_2$ MA-NHC-AgNPs in water and different organic solvents, (b) NaCl titration experiments with PMEO $_2$ MA-NHC-AgNPs and (c) citrate-capped AgNPs.



colloidal stability of PMEO₂MA—NHC—AgNPs was examined at the high concentration of the electrolyte, that is, NaCl, known to "salt out" polymer ligands^{57,58} and react with Ag. ^{55,59} PMED TO AGNE THE CONSTRUCTION OF THE CO

Our ligand-exchange method of polymer NHCs can further be extended to other NPs, for example, Ag nanowires (Ag NWs) and AuNPs. Ag NWs capped by polyvinylpyrrolidone (PVP) in water, as an example, can be modified with PS-NHCs (P3) at the interface of toluene and water (Figure 5). After stirring for 2 min, the phase transfer of Ag NWs was observed. The bottom layer containing PVP-Ag NWs became clear and the top layer with PS-NHC-Ag(I) turned gray and opaque after the exchange. In the UV-vis spectra, the LSPR peaks of PVP-AgNWs changed from 359 and 388 nm to 365 nm and 410 nm, which correspond to the quadrupole resonance excitation and transverse plasmon resonance, respectively. 60,61 The red shift was attributed to the increase in the refractive index of the surrounding medium of AgNPs. After ligand modification, the surrounding medium of AgNPs changed from water with a low refractive index to polymer ligands and toluene with a slightly high refractive index, leading to the LSPR shift to a longer wavelength. The TEM image in Figure 5c confirms that PVP-Ag NWs have a relatively large size in micrometer length with a diameter of ~97 nm. After the SHATERS WASHIFFER TIP BUTTERS ON ALL HUBBLES WHICH SHEET SHE About has been almostly a used in compared etablished in the citrate-capped ones with diameters of 3.5 and 14 nm. In the UV-vis spectra (Figure 5e), the citrate-capped 3.5 nm AuNPs have the LSPR of 513 nm that shift to 528 nm after the surface modification. Similarly, the LSPR of 14 nm AuNPs shift from 520 to 533 nm. All modified AuNPs had a single LSPR peak, and no aggregation was observed. The TEM images in Figures 5h,I show that all AuNPs can be modified without the changes in morphologies.

AgNPs usually have poor stability under oxidative conditions, for example, in the presence of peroxide. ⁶² H₂O₂ with a thermodynamic potential of 1.76 V relative to a standard hydrogen electrode is a strong oxidant and can etch AgNPs via $2Ag + H_2O_2 + 2H^+ \rightarrow 2H_2O + 2Ag^+$. Citratecapped AgNPs show oxidative etching in the presence of H₂O₂ (Figure 6a). With H₂O₂-to-Ag of 1:1 (mol), the LSPR peak intensity of AgNPs is decreased by about 42%. The LSPR peak had a blue shift of 5 nm, suggesting the oxidative etching of AgNPs to a smaller size. With the increase of H_2O_2 to H_2O_2 to-Ag of 3:1, AgNPs were completely etched, as can be seen in Figure 6b for the dispersion color change from pale yellow to colorless. The formation of Ag⁺ was confirmed by the addition of potassium iodine (KI, Figure S10). Addition of 20 μ L of 4 wt % KI solution led to immediate formation of a pale-yellow precipitate, AgI, due to the presence of Ag⁺ ions in the etching solution.

Polymer NHCs stabilize AgNPs more efficiently and prevent the NPs from oxidative etching by H_2O_2 . Figure 6c shows a typical H_2O_2 titration experiment of PMMA-NHC-AgNPs. When H_2O_2 was increased to 15 times (corresponding to H_2O_2 -to-Ag of 45:1, mol), the LSPR peak intensity decreased slightly due to the dilution, but no peak shift was seen. The photographs in Figure 6d show no solution color change for

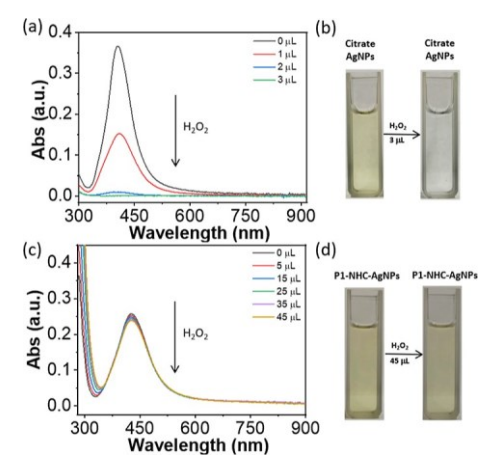


Figure 6. UV–vis spectra of AgNPs in the presence of H_2O_2 for (a) citrate-capped AgNPs and (c) PMMA–NHC–AgNPs. (b) Images showing the color change of the citrate AgNPs and (d) PMMA–NHC–AgNPs after H_2O_2 titration.

the PMMA–NHC–AgNPs with or without the presence of H_2O_2 . A similar stabilization effect can also be seen in $PMEO_2MA-NHC$ –AgNPs (Figure S11). Moreover, PMMA-NHC can prevent oxidative etching of Ag from not only H_2O_2 but also a high concentration of organic peroxide, such as tert-butyl hydrogen peroxide (TBHP) (Figure S12), and the competing small molecular ligands, that is, dithiothreitol (DTT) (Figure S13). The anti-corrosive properties of AgNPs coated with polymer NHCs are attributed to the strong binding of surface Ag atoms to NHCs that prevents their leaching under harsh conditions.

We compared the colloidal stability of AgNPs coated with polymer ligands but with different binding motifs, that is, NHC versus SH. We modified AgNPs with PS₁₂₀-NHC-Ag(I) (P3) and PS₁₃₄-SH (P4), both of which have a similar chain length. The oxidative etching of AgNPs was studied in the presence of H₂O₂ (H₂O₂-to-Ag of 20:1, mol) at 50 °C. While both PS (H2O₂-to-Ag o

The oxidative dissolution of AgNPs follows the pseudo second-order reaction when plotting the peak intensity against the reaction time. The apparent dissolution rate constants (k) for PS₁₂₀-NHC-AgNPs and PS₁₃₄-S-AgNPs are 0.011 and 7.99 L mol⁻¹ min⁻¹, respectively (Figure 7c). These values suggest that the dissolution rate of thiolate-stabilized AgNPs is 726-fold faster than that of PS₁₂₀-NHC-Ag. This confirms the high stability of polymer NHC-Ag binding. Additionally, we used X-ray photoelectron spectroscopy (XPS) to examine the residual polymer NHC ligands on the surface of AgNPs (Figure 7d). For PS₁₂₀-NHC-grafted AgNPs, the characteristic N 1S peak at 400.3 eV can be seen for nitrogen on NHCs before at spatial with H₂ Sugglifications.

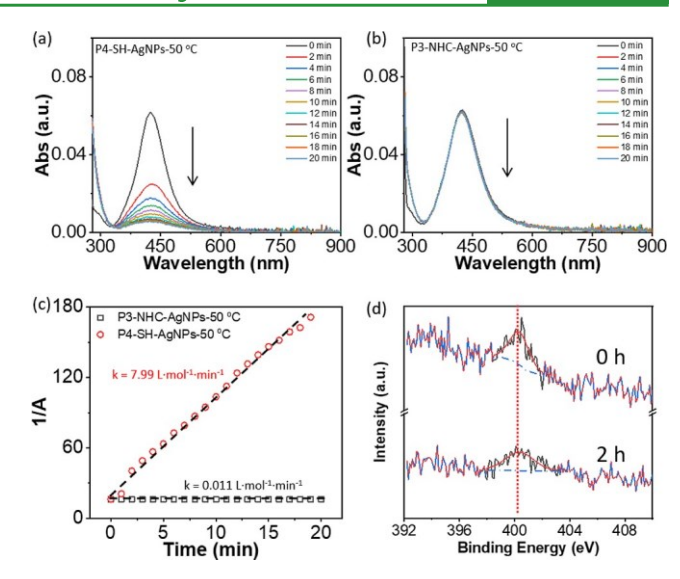


Figure 7. UV—vis spectra of polymer-modified AgNPs in the presence of H_2O_2 at $50\,^{\circ}$ C: (a) PS—SH—AgNPs and (b) PS—NHC—AgNPs. (c) Second-order kinetics fitting of the dissolution rate constants for PS—NHC—AgNPs (black, bottom) and PS—SH—AgNPs (red, top). (d) N 1S XPS spectra of PS—NHC—AgNPs before and after being treated with H_2O_2 for 2 h.

We further examined the peroxidase activity of polymer NHC-protected AgNPs. In the presence of Ag catalysts, the oxidation of 4-MEOP to p-benzoquinone with H₂O₂ was monitored by UV-vis using the absorption peak of 4-MEOP at 290 nm (Figure S15). The oxidation kinetics of 4-MEOP is typically first order. In the absence of the Ag catalyst, the autooxidation of 4-MEOP was very slow with an apparent k of 0.3 min^{-1} at 40 °C. Both PS_{120} -NHC-AgNPs and PS_{134} -S-AgNPs were active in catalyzing the oxidation of 4-MEOP. The reaction rate constants are 1.2 and 0.6 min⁻¹ in the presence of PS₁₂₀-NHC-AgNPs and PS₁₃₄-S-AgNPs, respectively (Figure 8a). We also compared the reaction catalyzed by citratecapped AgNPs and polyvinylpyrrolidone (PVP)-modified AgNPs. The k values of the two reactions were 0.33 and 0.41 min⁻¹, respectively, very close to the auto-oxidation of 4-MEOP. Not surprisingly, citrate-capped AgNPs and PVPmodified AqNPs were unstable in the presence of H₂O₂. Therefore, no catalytic behaviors were seen in both cases. On the contrary, PS₁₂₀-NHC-AgNPs and PS₁₃₄-S-AgNPs were much more stable, and they could catalyze the oxidation of 4-MEOP. To further examine the difference and the importance of the binding motif, the reaction kinetics were measured under different temperatures in the range of 20-50 °C (Table S1 and Figure 8b,c). As shown in Figure 8d, the reaction rate increases along with the temperature as a typical Arrhenius behavior. The activation energy of 4-MEOP oxidation catalyzed by PS_{120} -NHC-AgNPs and PS_{134} -S-AgNPs is 58.9 and 62.5 KJ mol⁻¹, respectively. This suggests that AgNPs grafted by the two polymers show very similar catalytic characteristics, essentially with similar reaction pathways. Therefore the thife renominactivity is attributed to the toin ding binding scheme, the strong σ election donation of NHCs makes AgNPs electron rich, which facilitates the reduction of H₂O₂ to hydroxyl radicals of OH⁶⁴ and oxidation of phenol to p-benzoquinone.65

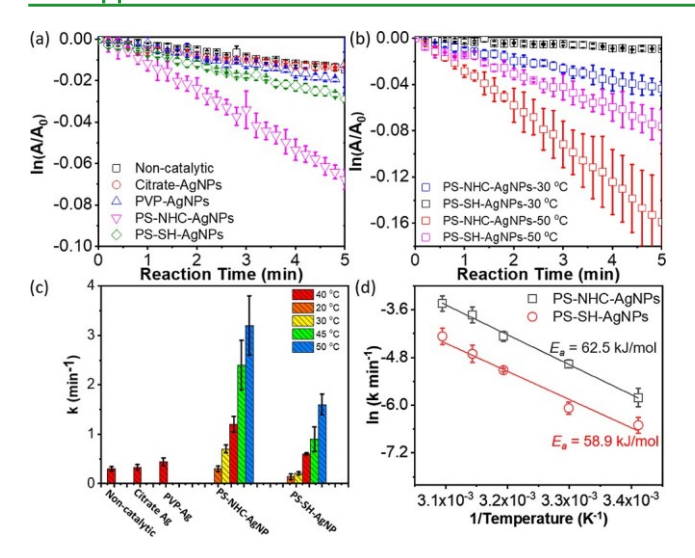


Figure 8. (a) Pseudo first-order kinetics of the 4-MEOP oxidation reaction with different catalysts. (b) Reaction kinetics of 4-MEOP oxidation with PS-NHC-AgNPs and PS-SH-AgNPs at 30 and 50 °C, respectively. (c) Dependence of the rate constant (k) vs different frame and the first points and PS-SH-AgNPs at 20-50 °C.

3. CONCLUSIONS

In summary, we developed a facile "grafting-to" method to add polymer NHCs to metal NPs through trans-metalation with polymeric NHC-Ag(I). Three imidazolium-terminated polymers, including PS, PMMA, and PMEO₂MA, were first prepared through ATRP, and polymeric NHC-Ag(I) were BINGLEAN CONTROLL AND THE PROPERTY OF THE PROP through an interfacial ligand exchange at the interface of toluene and water. Within a 2 min modification, the grafting density of PMMA-NHC-AqNPs is ~0.1 chains nm⁻². Our method could be extended to other metal NPs, such as AuNPs and AgNWs, regardless of the NP size and composition. Polymer NHC-modified AgNPs were exceptionally stable under thermal, highly oxidative, and reactive (e.g., NaCl) conditions. In the presence of H₂O₂ at 50 °C, PS-NHC that Post had a structure that present the by of a strictly do than MEGIEsea A grups det his applion into ceval lingues three least all yrings the reatal yrings the reatal yrings three seasily its reactive than the citrate - and PVP-AgNPs and 2 times more reactive than the PS-S-AgNPs. The polymer NHC coating demonstrated here offers a general approach to metal NP stabilization against aggregation, providing a unique way of studying single NP behaviors for important applications.

4. EXPERIMENTAL SECTION

4.1. Chemicals and Materials. All chemicals were purchased from Aldrich unless otherwise noted. Styrene (99%), methyl methacrylate (MMA), and di(ethylene glycol) methyl ether methacrylate (MEO₂MA) were passed through a basic aluminum oxide column prior to use. N,N,N, N', N'-Pentamethyl diethylenetriamine (PMDETA, > 99%), %), 2-bromo-2-methylpropionyl bromide (BMPB, 98%), copper(I) bromide (CuBr, 99.999% trace metal basis), anisole (anhydrous, 99.7%), imidazole (99%), dimethylformamide (DMF, 99.8%), methanol (99.8%), tetrahydrofuran (THF, anhydrous, 99.9%), hexane (anhydrous, 95%), dichloromethane (DCM, \geq 99.9%), iodomethane (CH₃I), silver oxide (Ag₂O), 4-methoxyphenol

(98.0%), 1,4-dioxane (99.8%), ascorbate acid, and hydrogen peroxide (30 wt % aqueous solution) were used as received. Sodium citrate tribasic dihydrate (>99.0%) and silver nitrate (AgNO $_3$) (>98.0%) were purchased from Alfa Aesar. The ultra-pure water was distilled with a High-Q distillation system (model # 103S).

4.2. Synthesis of an Imidazole-Containing ATRP Initiator. 2-(1-Imidazole-1-yl) ethanol (IM-OH) was synthesized by a coupling reaction between imidazole (IM) and 2-chloroethanol as reported in a previous literature. IM (12.5 g, 0.18 mmol), 2-chloroethanol (14.7 g, 0.18 mmol), and sodium hydroxide (7.3 g, 0.18 mmol) were mixed into 50 mL of 1,4 dioxane in a 250 mL round-bottom flask. The solution was stirred at 35 °C overnight. After cooling down to room temperature, the solid precipitate was separated by filtration. The recovered liquid was poured into 200 mL of cold ethyl acetate under stirring. The mixture was incubated at an ice bath for 30 min to recrystallize the product. The solid crystal was washed with 100 mL of good at the cold at

The imidazole-containing ATRP initiator was prepared by coupling IM-OH and the bromide-containing precursor of BMPB. Typically, IM-OH (2 g, 0.018 mmol) and triethylamine (TEA) (18 g, 0.018 mmol) were mixed with 100 mL of dry DCM to a 250 mL roundbottom flask under stirring in an ice bath. The mixture was degassed and purged with N2 for 30 min. BMPB (4 g, 0.018 mmol) was dissolved in 5 mL of dry DCM, and the solution was added dropwise to the reaction mixture in 30 min with a N2 flow. The reaction mixture was stirred overnight. After reaction, the reaction mixture was extracted with saturated sodium bicarbonate (NaHCO₃) solution four times. All DCM layers were collected and combined. The solution was dried with anhydrous Na₂SO₄ for 4 h. After the removal of DCM by a rotary vapor under vacuum, the ATRP initiator of IM-Br was obtained as an oily yellow liquid. ¹H NMR (400 MHz CDCl₃): δ $(ppm) = 7.54 (s, 1H, -NHC \odot CHN-), 7.08 (s, 1H, -CH-IM-), 7.0$ (s, 1H, -CH-IM-), 4.42 (t, 2H, -CH₂-), 4.26 (s, 2H, -CH₂-), and 1.9 (s, 6H, -CH₃).

4.3. Synthesis of IM- and NHC-Terminated Polymers. 4.3.1. Synthesis of PMMA-IM. The IM-terminated homopolymer of PMMA was synthesized using ATRP with IM-Br as the initiator. Typically, MMA (5 g, 50 mmol) and CuBr (0.072 g, 0.5 mmol) were mixed with 1 mL of anhydrous anisole. The mixture was degassed and purged with N₂ for 5 min. Then, PMDETA (0.17 g, 0.5 mmol) was added to the reaction mixture. The reaction solution was continuously purged with N₂ for another 15 min. IM-Br (0.13 g, 0.5 mmol) dissolved in 0.5 mL of anhydrous anisole was added to the solution. The mixture was further purged with N₂ for 20 min. After the solution was stirred at room temperature for 30 min. the reaction mixture was exposed to air, and 5 mL of DCM was added to quench the polymerization. The solution mixture was passed through a silica gel column with DCM as an eluent to remove Cu residues. The solution was then transferred to another round-bottom flask. Next, 3 mL of CH₃I was added to the polymer solution mixture overnight. After concentrating under vacuum, the polymer was precipitated in hexane three times. PMMA-IM was collected and dried under vacuum for 24 h. The yielded polymer has a M_n of 31.2 kg/mol, and the dispersity is 1.2 measured by gel permission chromatography (GPC). The number of repeat units was calculated to be 258 from ¹H NMR by using the protons at 9.6 ppm as the internal standard.

4.3.2. Synthesis of PS-IM. The IM-terminated homopolymer of PS was synthesized using ATRP with IM-Br as the initiator. Typically, St (5 g, 51.2 mmol) and CuBr (0.15 g, 1.03 mmol) were mixed with 1 mL of anhydrous anisole. The mixture was degassed and purged with N_2 for 5 min. PMDETA (0.18 g, 1.03 mmol) was added to the reaction mixture. Then, the reaction solution was continuously purged with N_2 for another 15 min. IM-Br (0.27 g, 1.03 mmol) in 0.5 mL of anhydrous anisole was added to the reaction solution. Then, it was further purged with N_2 for 20 min. After the solution was stirred at room temperature for 30 min, the reaction solution was transferred in

a preheated oil bath at 80 °C for 12 h. After the polymerization, the reaction mixture was exposed to air, and 5 mL of DCM was added to quench the polymerization. The polymer solution was passed through a silica gel column with DCM as the eluent to remove the Cu residues. The solution was transferred to another round-bottom flask. Next, 3 mL of CH $_3$ I was added to the polymer solution mixture and stirred overnight. After the reaction, the solution was concentrated under vacuum. The polymer was precipitated in methanol three times. PS-IM was collected and dried under vacuum for 24 h. The yield polymer has a M_n of 11.1 kg/mol, and the dispersity is 1.2 measured by GPC. The number of repeat units was calculated to be 120 from $^1\mathrm{H}$ NMR by using the protons at 9.6 ppm as the internal standard.

4.3.3. Synthesis of PMEO₂MA-IM. The IM-terminated homopolymer of PMEO₂MA was synthesized using ATRP with IM-Br as the initiator. Typically, MEO₂MA (6 g, 31.9 mmol) and CuBr (151.6 q. 1.06 mmol) were mixed with 1 mL of anhydrous anisole. The mixture was degassed and purged with N2 for 5 min. PMDETA (0.39 g, 2.1 mmol) was added to the reaction mixture. It was continuously purged with N₂ for another 15 min. IM-Br (0.28 g, 1.1 mmol) in 0.5 mL of anhydrous anisole was added to the reaction solution. Then, it was further purged with N₂ for 20 min. The solution was stirred at room temperature for 30 min. After the polymerization, the reaction mixture was exposed to air, and 5 mL of DCM was added to quench the reaction. The polymer solution was passed through a silica gel column with DCM as the eluent to remove the Cu residues. The resulted solution was transferred to another round-bottom flask. Next, 3 mL of CH3I was added to the polymer solution mixture and then stirred overnight. After the reaction, the solution was concentrated under vacuum. It was precipitated in hexane three times. The viscous liquid of PMEO₂MA-IM was collected and dried under vacuum for 24 h. The yield polymer has a M_n of 32.4 kg/mol, and the polymer dispersity is 1.2 measured by GPC. The number of repeat units was calculated to be 145 from ¹H NMR by using the protons at 9.6 ppm as the internal standard.

4.3.4. Synthesis of NHC-Ag-Terminated Polymers. NHC-Ag(I)-terminated polymers were prepared by making the complexation with polymeric imidazolium and Ag₂O. For example, 500 mg of PMMA₂₅₈-IM (19.3 µmol of imidazole) was dissolved into 40 mL of DCM to a 100 mL round-bottom flask. Then, the flask was fully covered by an aluminum foil to avoid the light irritation. Ag₂O (6.6 mg, 28.5 µmol) was added to the reaction flask. The reaction was sealed and stirred for 24 h. After the reaction, the polymer solution was passed through a silica gel column with DCM as the eluent to remove Ag₂O residues. Free prediction was sealed and through was decollected and then dried under vacuum for 24 h. The preparations of PEO₂MA₁₄₅-NHC-Ag(I) and PS₁₂₀-NHC-Ag(I) were followed up by similar procedures.

4.4. Synthesis of Various NPs with Ag and Au. *4.4.1. Synthesis of AgNPs.* AgNPs were synthesized according to a previously reported literature with minor modifications. ⁵² Deionized (DI) water (47.5 mL) was added to a boiled water bath. AgNO $_3$ (2.5 mg) in 25 μ L of water was mixed with 1 mL of sodium citrate solution (1 wt %). The solution was incubated for 5 min at room temperature. Then, 50 μ L of 0.1 M ascorbic acid solution was injected to boiled DI water. After 1 min, AgNO $_3$ and sodium citrate solution were quickly injected to the reaction. The solution color was changed from colorless to yellow. The reaction was further boiled and stirred for another 1 h. The average size of AgNPs is 27 nm.

4.4.2. Synthesis of PVP-AgNWs. AgNWs were synthesized according to the reported method. 66 PVP (0.2 g) was dissolved to the reported method. 66 PVP (0.2 g) was dissolved to the reported method. 69 PVP (0.2 g) was dissolved to the reported method. 69 PVP (0.2 g) was dissolved to the reported tunder of the region of the reported region of the reported region of the reported method. 69 PVP (0.2 g) was dissolved to the reported tunder of the region o

4.4.3. Synthesis of AuNPs. Citrate AuNPs (14 nm) were synthesized according to the previous literature. HAuCl₄ (100 mg) was dissolved into 1 L of DI water, and the reaction was placed into a preheated water bath (100 °C). Sodium citrate solution (1 wt %) was quickly injected into the HAuCl₄ solution. Then, it was allowed to react for 30 min. AuNPs (14 nm) were collected by centrifuging the solution at 11000 rpm. The average size of AuNPs was confirmed by the TEM image.

Citrate AuNPs (3.5 nm) were prepared with 5 mg of HAuCl $_4$ and 3.7 mg of sodium citrate in a 100 mL aqueous solution. Then, 1.5 mL of freshly prepared 0.1 M of NaBH $_4$ was injected into the above solution under stirring. The solution changed from colorless to orange immediately with further stirring for 4 h. The average size (3.5 nm) of AuNPs was confirmed by the TEM image.

4.5. Surface Modification of AgNPs. The surface modification of AgNPs was carried out through a biphasic ligand exchange. For example, 5 mg of PMMA₂₅₈-NHC-Ag(I) was dissolved into 5 mL of toluene. Then, 10 mL of AgNP dispersion was transferred to a 15 mL glass vial, and the polymer solution was poured into the same vial. The solution mixture was stirred for 2 min until all the AgNPs were transferred to the polymer solution phase. PMMA-NHC-AgNP dispersion was collected and diluted with toluene to 20 mL. PMMA-NHC-AgNP dispersions were centrifuged four times to remove the free polymers. The collected PMMA-NHC-modified AgNPs were solution phase. The collected PMMA-NHC-modified AgNPs were solvents of the AgNPs with PS-NHC-Ag(I) and PMEO₂MA-NHC-Ag(I) was followed up similar procedures.

As a reference, AgNPs grafted by PS_{134} -SH was achieved by a

single-phase ligand exchange. Typically, 5 mg of PS $_{134}$ -SH was dissolved in 5 mL of DMF. Then, 5 mL of citrate-capped AgNPs was concentrated to 100 μ L by centrifuging the solution at 8500 rpm for solution. Whe represents the incubated at room temperature for 2 h. To remove the free polymers, the dispersion was centrifuged four times. Finally, PS $_{134}$ -SH-modified AgNPs were redispersed to different organic solvents, such as THF and DMF.

4.6. Stability Tests of Polymer NHC-Modified AgNPs. 4.6.1. Oxidative Stability Test with Peroxide. The oxidative stability was examined by H_2O_2 titration while monitoring the changes of LSPR in UV-vis spectroscopy. For example, 3 mL of PMMA-

NHC-AgNPs (0.02 mg mL) was injected to a 3.5 mL quartz cuvette. Then, 5 μ L of 30 wt % H_2O_2 was continuously added to AgNP dispersion and then mixed well. The UV-vis spectrum was selecting after that additional evers A-midified examples the oxidative temperature, 5 μ L of 30 wt % H_2O_2 was added to AgNP dispersion at 50 °C. The LSPR change was recorded by UV-vis spectroscopy every 2 min. Similarly, the organic peroxide stability was examined with PMMA-NHC-AgNPs by titrating TBHP at room temperature. stabilities be an example of the continuous peroxide stability was examined with PMMA-NHC-AgNPs by titrating TBHP at room temperature. stabilities be an example of the continuous peroxide stability was examined by the continuous peroxide of the continuous peroxide and the continuous peroxide stability was examined by the continuous peroxide and the c

4.7. Oxidation of 4-Methoxyphenol. The catalytic activity of NPs under the highly oxidative condition was evaluated using the oxidation 4-MEOP as a model reaction. Typically, 30 μ L of AgNPs (0.2 mg mL $^{-1}$) and 5 μ L of 30 wt % H₂O₂ were added to 3 mL of Tris buffer solution (pH $_{\rm e}$ =8). Then, 50 μ L of the 4-MEOP solution in ethanol (1 mg mL $^{-1}$) was added into the above solution to trigger the reaction under 40 $^{\circ}$ C. The reaction kinetics were monitored by the in situ reduction of UV–vis absorbance intensity at 290 nm, which corresponds to the absorbance of 4-MEOP.

To evaluate the activation energy of the oxidation 4-MEOP catalyzed by PS-modified AgNPs, the reaction was carried out with the same conditions except at varying temperatures. The temperature

ranged from 20 to 50 $^{\circ}$ C. The reaction kinetics was monitored by UV-vis spectra. In addition, the reaction behavior follows up the pseudo first-order reaction kinetics. The obtained reaction rates were plotted with different temperatures. To fit Arrhenius plots, the Arrhenius plot (see below) of $\ln k$ versus 1/T was used as

$$\ln k = -\frac{E_{\rm a}}{RT} + \ln A$$

where k is the rate constant, E_a is the activation energy for the reaction, R is the gas constant, T is the absolute temperature (K), and A is the pre-exponential factor. The plot was built up by $\ln k$ versus 1/T. With the linear fitting, the slope can be used to calculate E_a .

ASSOCIATED CONTENT

Supporting Information

The Supporting Information is available free of charge at https://pubs.acs.org/doi/10.1021/acsami.2c17706.

Detailed synthesis procedure, characterization details of polymers, more electron microscopic characterization, calculation of grafting density, UV-vis absorption spectroscopy, and catalytic performance (PDF)



AUTHOR INFORMATION

Corresponding Author

Jie He — Department of Chemistry and Polymer Program, Institute of Materials Science, University of Connecticut, Storrs, Connecticut 06269, United States; ● orcid.org/0000-0003-0252-3094; Email: jie.he@uconn.edu

Authors

Zichao Wei — Department of Chemistry, University of Connecticut, Storrs, Connecticut 06269, United States; orcid.org/0000-0001-5818-5077

Kayceety Mullaj — Department of Chemistry, University of Connecticut, Storrs, Connecticut 06269, United States
Aleisha Price — Department of Chemistry, University of Connecticut, Storrs, Connecticut 06269, United States
Kecheng Wei — Department of Chemistry, Brown University, Providence, Rhode Island 02912, United States
Qiang Luo — Department of Chemistry, University of Connecticut, Storrs, Connecticut 06269, United States
Srinivas Thanneeru — Department of Chemistry, University of Connecticut, Storrs, Connecticut 06269, United States
Shouheng Sun — Department of Chemistry, Brown University, Providence, Rhode Island 02912, United States

Complete contact information is available at: https://pubs.acs.org/10.1021/acsami.2c17706

Notes

The authors declare no competing financial interest.

ACKNOWLEDGMENTS

J.H. is grateful for the continuous financial support from the University of Connecticut through the VPR-REP program and the National Science Foundation (CHE-2102245). The electron microscopy studies were performed using the facilities in the Bioscience Electron Microscopy Laboratory at the University of Connecticut.

REFERENCES

(1) Lin, J.; Wang, S.; Huang, P.; Wang, Z.; Chen, S.; Niu, G.; Li, W.; He, J.; Cui, D.; Lu, G.; Chen, X.; Nie, Z. Photosensitizer-Loaded Gold Vesicles with Strong Plasmonic Coupling Effect for Imaging-Guided

Photothermal/Photodynamic Therapy. ACS Nano 2013, 7, 5320-5329

- (2) Liu, Z.; Cai, W.; He, L.; Nakayama, N.; Chen, K.; Sun, X.; Chen, X.; Dai, H. Vivo Biodistribution and Highly Efficient Tumour Targeting of Carbon Nanotubes in Mice. *Nat. Nanotechnol.* 2007, 2, 47-52.
- (3) Yang, K.; Zhang, S.; He, J.; Nie, Z. Polymers and Inorganic Nanoparticles: A Winning Combination Towards Assembled Nanostructures for Cancer Imaging and Therapy. *Nano Today* 2021, *36*, 101046.
- (4) He, J.; Huang, X.; Li, Y.-C.; Liu, Y.; Babu, T.; Aronova, M. A.; Wang, S.; Lu, Z.; Chen, X.; Nie, Z. Self-Assembly of Amphiphilic Charmonic More lety-specific in Selective Solvents. *J. Am.*
- off-)ariy Gno-flama. Nai Melahides T. Able One An Interpret 2017, Self, Argenthly (6) Zhang, L.; Wei, Z.; Thanneeru, S.; Meng, M.; Kruzyk, M.; Ung, G.; Liu, B.; He, J. A Polymer Solution to Prevent Nanoclustering and Improve the Selectivity of Metal Nanoparticles for Electrocatalytic Co2 Reduction. Angew. Chem., Int. Ed. 2019, 58, 15834—15840.
- (7) Zhang, L.; Wei, Z.; Meng, M.; Ung, G.; He, J. Do Polymer Ligands Block the Catalysis of Metal Nanoparticles? Unexpected Immeritarisem. A Evizying Manifes-insomeroring Catalytic Activity. J.
- (8) Chen, Y.; Wang, Z.; Harn, Y. W.; Pan, S.; Li, Z.; Lin, S.; Peng, J.; Zhang, G.; Lin, Z. Resolving Optical and Catalytic Activities in Thermoresponsive Nanoparticles by Permanent Ligation with Temperature-Sensitive Polymers. *Angew. Chem., Int. Ed.* 2019, 58, 11910–11917.
- (9) Wu, S.; Wang, T.; Xu, H. Regulating Heterogeneous Catalysis of Gold Nanoparticles with Polymer Mechanochemistry. *ACS Macro Lett.* 2020, 9, 1192–1197.
- (10) Ansar, S. M.; Kitchens, C. L. Impact of Gold Nanoparticle stabilizing Ligand வரு நூக்கு பூர்க்கு புக்கு புக்
- (11) Wang, M.; Pang, X.; Zheng, D.; He, Y.; Sun, L.; Lin, C.; Lin, Z. Nonepitaxial Growth of Uniform and Precisely Size-Tunable Core/Shell Nanoparticles and Their Enhanced Plasmon-Driven Photocatalysis. *J. Mater. Chem. A* 2016, *4*, 7190–7199.
- (12) Chen, Y.; Yang, D.; Yoon, Y. J.; Pang, X.; Wang, Z.; Jung, J.; He, Y.; Harn, Y. W.; He, M.; Zhang, S.; Zhang, G.; Lin, Z. Hairy Uniform Permanently Ligated Hollow Nanoparticles with Precise Dimension Control and Tunable Optical Properties. *J. Am. Chem. Soc.* 2017, 139, 12956–12967.
- (13) Que, Y.; Feng, C.; Zhang, S.; Huang, X. Stability and Catalytic Activity of Peg-B-Ps-Capped Gold Nanoparticles: A Matter of Ps Chain Length. *J. Phys. Chem. C* 2015, *119*, 1960–1970.
- (14) He, J.; Liu, Y.; Babu, T.; Wei, Z.; Nie, Z. Self-Assembly of Inorganic Nanoparticle Vesicles and Tubules Driven by Tethered Linear Block Copolymers. *J. Am. Chem. Soc.* 2012, 134, 11342—11345
- RUBTHS WIF, Av. FSWAF. ASSEKHUNN ACOP V METAL: FSWAF AND SEEKHUNN ACOP V METAL: FSWAF AND SEEKHUNN ACOP V METAL: A
- (16) Roth, P. J.; Boyer, C.; Lowe, A. B.; Davis, T. P. Raft Polymerization and Thiol Chemistry: A Complementary Pairing for Implementing Modern Macromolecular Design. *Macromol. Rapid Commun.* 2011, 32, 1123–1143.
- (17) Yang, Y.; Yi, C.; Duan, X.; Wu, Q.; Zhang, Y.; Tao, J.; Dong, W.; Nie, Z. Block-Random Copolymer-Micellization-Mediated Enemation 2001 Polymering of Galomes on Gold Nanoparticles. *J. Am.*
- (18) Duan, H.; Luo, Q.; Wei, Z.; Lin, Y.; He, J. Symmetry-Broken Patches on Gold Nanoparticles through Deficient Ligand Exchange. *ACS Macro Lett.* 2021, *10*, 786–790.
- (19) Yi, C.; Liu, H.; Zhang, S.; Yang, Y.; Zhang, Y.; Lu, Z.; Kumacheva, E.; Nie, Z. Self-Limiting Directional Nanoparticle Bonding Governed by Reaction Stoichiometry. *Science* 2020, 369, 1369–1374.

- (20) Li, F.; Zhang, H.; Dever, B.; Li, X.-F.; Le, X. C. Thermal Stability of DNA Functionalized Gold Nanoparticles. *Bioconjugate Chem.* 2013, 24, 1790–1797.
- (21) Ling, X.; Schaeffer, N.; Roland, S.; Pileni, M.-P. Superior ยิงพระลาเรียกฟังหากปีปิสยาการแระเรียกพระเรา
- (22) Shen, H.; Tian, G.; Xu, Z.; Wang, L.; Wu, Q.; Zhang, Y.; Teo, B. K.; Zheng, N. N-Heterocyclic Carbene Coordinated Metal Nanoparticles and Nanoclusters. *Coord. Chem. Rev.* 2022, 458, 214425.
- (23) Smith, C. A.; Narouz, M. R.; Lummis, P. A.; Singh, I.; Nazemi, A.; Li, C.-H.; Crudden, C. M. N-Heterocyclic Carbenes in Materials Chemistry. *Chem. Rev.* 2019, *119*, 4986–5056.
- (24) Duan, H.; Lin, Y.; He, J.Polymeric N-Heterocyclic Carbenes to Functionalize Plasmonic Metal Nanoparticles. *World Scientific Reference on Plasmonic Nanomaterials*; Dimensons, 2022, pp 409–432.
- (25) Nosratabad, N. A.; Jin, Z.; Du, L.; Thakur, M.; Mattoussi, H. N-Heterocyclic Carbene-Stabilized Gold Nanoparticles: Mono-Versus Multidentate Ligands. *Chem. Mater.* 2021, *33*, 921–933.
- (26) Sun, N.; Zhang, S. T.; Simon, F.; Steiner, A. M.; Schubert, J.; Du, Y.; Qiao, Z.; Fery, A.; Lissel, F. Poly (3-Hexylthiophene) S Functionalized with N-Heterocyclic Carbenes as Robust and Conductive Ligands for the Stabilization of Gold Nanoparticles. *Angew. Chem., Int. Ed.* 2021, 60, 3912–3917.
- (27) Man, R. W. Y.; Li, C.-H.; MacLean, M. W. A.; Zenkina, O. V.; Zamora, M. T.; Saunders, L. N.; Rousina-Webb, A.; Nambo, M.; Crudden, C. M. Ultrastable Gold Nanoparticles Modified by Bidentate N-Heterocyclic Carbene Ligands. *J. Am. Chem. Soc.* 2018, 140, 1576–1579.
- (28) Inayeh, A.; Groome, R. R.; Singh, I.; Veinot, A. J.; de Lima, F. Geteliogoria. Darbeneden Au M11McNan Commune 2020 թ. բողջիկ 054 գ
- (29) Cao, Z.; Kim, D.; Hong, D.; Yu, Y.; Xu, J.; Lin, S.; Wen, X.; Nichols, E. M.; Jeong, K.; Reimer, J. A.; Yang, P.; Chang, C. J. A Molecular Surface Functionalization Approach to Tuning Nanoparticle Electrocatalysts for Carbon Dioxide Reduction. *J. Am. Chem. Soc.* 2016, *138*, 8120–8125.
- (30) Cao, Z.; Derrick, J. S.; Xu, J.; Gao, R.; Gong, M.; Nichols, E. M.; Smith, P. T.; Liu, X.; Wen, X.; Copéret, C.; Chang, C. J. Chelating N-Heterocyclic Carbene Ligands Enable Tuning of Electrocatalytic Co2 Reduction to Formate and Carbon Monoxide: Surface Organometallic Chemistry. *Angew. Chem., Int. Ed.* 2018, 130, 5075–5079.
- C(31)BG(65)-ZaraqovataAr.; Aereconhayaræte Martinbellare Gunit. Am. Tailoring Graphene-Supported Ru Nanoparticles by Functionalization with Pyrene-Tagged N-Heterocyclic Carbenes. Catal. Sci. Technol. 2022, 12, 1257—1270.
- (32) Ott, L. S.; Cline, M. L.; Deetlefs, M.; Seddon, K. R.; Finke, R. G. Nanoclusters in Ionic Liquids: Evidence for N-Heterocyclic Garbaner Frinking from Ionic Liquids from
- (33) Vignolle, J.; Tilley, T. D. N-Heterocyclic Carbene-Stabilized Coldminanopagicles and Their Assembly into 3d Superlattices. Chem.
- (34) Bridonneau, N.; Hippolyte, L.; Mercier, D.; Portehault, D.; Desage-El Murr, M.; Marcus, P.; Fensterbank, L.; Chanéac, C.; Ribot, F. N-Heterocyclic Carbene-Stabilized Gold Nanoparticles with Tunable Sizes. *Dalton Trans.* 2018, 47, 6850–6859.
- (35) Richter, C.; Schaepe, K.; Glorius, F.; Ravoo, B. J. Tailor-Made
- (36) Song, S. G.; Satheeshkumar, C.; Park, J.; Ahn, J.; Premkumar, T.; Lee, Y.; Song, C. N-Heterocyclic Carbene-Based Conducting Polymer-Gold Nanoparticle Hybrids and Their Catalytic Application. *Macromolecules* 2014, 47, 6566-6571.
- (37) Ru hling, A.; Schaepe, K.; Rakers, L.; Vonhören, B.; Tegeder, P.:
- Ravoo, B. J.; Glorius, F. Modular Bidentate Hybrid Nhc-Thioether

- Ligands for the Stabilization of Palladium Nanoparticles in Various Solvents. *Angew. Chem., Int. Ed.* 2016, *55*, 5856–5860.
- (38) Ye, R.; Zhukhovitskiy, A. V.; Kazantsev, R. V.; Fakra, S. C.; Wickemeyer, B. B.; Toste, F. D.; Somorjai, G. A. Supported Au Nanoparticles with N-Heterocyclic Carbene Ligands as Active and Stable Heterogeneous Catalysts for Lactonization. *J. Am. Chem. Soc.* 2018, 140, 4144–4149.
- (39) Soulé, J.-F.; Miyamura, H.; Kobayashi, S. Copolymer-Incarcerated Nickel Nanoparticles with N-Heterocyclic Carbene Precursors as Active Cross-Linking Agents for Corriu-Kumada-Tamao Reaction. J. Am. Chem. Soc. 2013, 135, 10602–10605.
- (40) Ferry, A.; Schaepe, K.; Tegeder, P.; Richter, C.; Chepiga, K. M.; Ravoo, B. J.; Glorius, F. Negatively Charged N-Heterocyclic Carbene-Stabilized Pd and Au Nanoparticles and Efficient Catalysis in Water. *ACS Catal.* 2015. *5*. 5414–5420.
- (41) Crudden, C. M.; Horton, J. H.; Narouz, M. R.; Li, Z.; Smith, C. A.; Munro, K.; Baddeley, C. J.; Larrea, C. R.; Drevniok, B.; Thanabalasingam, B.; McLean, A. B.; Zenkina, O. V.; Ebralidze, I. I.; She, Z.; Kraatz, H.-B.; Mosey, N. J.; Saunders, L. N.; Yagi, A. Simple Direct Formation of Self-Assembled N-Heterocyclic Carbene Monolayers on Gold and Their Application in Biosensing. *Nat. Commun.* 2016, 7, 12654.
- (42) Engel, S.; Fritz, E.-C.; Ravoo, B. J. New Trends in the Figure Partie of the Figure of the Figu
- (44) Hurst, E. C.; Wilson, K.; Fairlamb, I. J. S.; Chechik, V. N-Heterocyclic Carbene Coated Metal Nanoparticles. *New J. Chem.* 2009, 33, 1837–1840.
- (45) de los Bernardos, M. D.; Pérez-Rodríguez, S.; Gual, A.; Claver, C.; Godard, C. Facile Synthesis of Nhc-Stabilized Ni Nanoparticles and Their Catalytic Application in the Z-Selective Hydrogenation of Alkynes. *Chem. Commun.* 2017, *53*, 7894–7897.
- (46) Veinot, A. J.; Al-Rashed, A.; Padmos, J. D.; Singh, I.; Lee, D. S.; Narouz, M. R.; Lummis, P. A.; Baddeley, C. J.; Crudden, C. M.; Horton, J. H. N-Heterocyclic Carbenes Reduce and Functionalize Copper Oxide Surfaces in One Pot. *Eur. J. Chem.* 2020, 26, 11431–11434.
- (47) Thanneeru, S.; Ayers, K. M.; Anuganti, M.; Zhang, L.; Kumar, C. V.; Ung, G.; He, J. N-Heterocyclic Carbene-Ended Polymers as Surface Ligands of Plasmonic Metal Nanoparticles. *J. Mater. Chem. C* 2020, *8*, 2280–2288.
- (48) Wang, Z.; Tzouras, N. V.; Nolan, S. P.; Bi, X. Silver N-Heterocyclic Carbenes: Emerging Powerful Catalysts. *Trends Chem* 2021. 3, 674–685.
- (49) Wang, H. M.; Lin, I. J. Facile Synthesis of Silver (I)— Carbene Complexes. Useful Carbene Transfer Agents. *Organometallics* 1998, 17, 972–975.
- (50) Burling, S.; Mahon, M. F.; Reade, S. P.; Whittlesey, M. K. Herthalland Cationia in Horizotal Anti-Heritage Wells. Sarty-net Corporates
- (51) Wang, G.; Pecher, L.; Frenking, G.; Dias, H. V. R. Vinyltrifluoroborate Complexes of Silver Supported by N-Heterocyclic Carbenes. *Eur. J. Inorg. Chem.* 2018, 2018, 4142–4152.
- (52) Li, H.; Xia, H.; Ding, W.; Li, Y.; Shi, Q.; Wang, D.; Tao, X. Synthesis of Monodisperse, Quasi-Spherical Silver Nanoparticles with Sizes Defined by the Nature of Silver Precursors. *Langmuir* 2014, *30*, 2498–2504.
- (53) Liu, B.; Thanneeru, S.; Lopes, A.; Jin, L.; McCabe, M.; He, J. Surface Engineering of Spherical Metal Nanoparticles with Polymers toward Selective Asymmetric Synthesis of Nanobowls and Janus-Type Dimers. *Small* 2017, *13*, 1700091.
- (54) Hu, L.; Wang, Y.; Yin, Q.; Du, K.; Yin, Q. Multiple Morphologies of a Poly(Methyl Methacrylate)-Block-Poly(N,N-Dimethyl Aminoethyl Methacrylate) Copolymer with Ph-Responsiveness and Thermoresponsiveness. J. Appl. Polym. Sci. 2019, 136, 47972.

- H. 55). ZDangathve Vinuele alteng, and Cerrowth; Sujanus Prope Minely, Roj and Mnox-Agi Nanoparticles. Nanoscale 2019, 11, 15147-15155.
- (56) Nosratabad, N. A.; Jin, Z.; Du, L.; Thakur, M.; Mattoussi, H. N-Heterocyclic Carbene-Stabilized Gold Nanoparticles: Mono-Versus Multidentate Ligands. Chem. Mater. 2021, 33, 921-933.
- (57) Radziuk, D.; Skirtach, A.; Sukhorukov, G.; Shchukin, D.; Möhwald, H. Stabilization of Silver Nanoparticles by Polyelectrolytes and Poly(Ethylene Glycol). Macromol. Rapid Commun. 2007, 28,
- (58) Huynh, K. A.; Chen, K. L. Aggregation Kinetics of Citrate and Polyvinylpyrrolidone Coated Silver Nanoparticles in Monovalent and Divalent Electrolyte Solutions. Environ. Sci. Technol. 2011, 45, 5564-
- (59) Wiley, B.; Herricks, T.; Sun, Y.; Xia, Y. Polyol Synthesis of Silver Nanoparticles: Use of Chloride and Oxygen to Promote the Formation of Single-Crystal, Truncated Cubes and Tetrahedrons. Nano Lett. 2004, 4, 1733-1739.
- (60) Azani, M. R.; Hassanpour, A. Synthesis of Silver Nanowires with Controllable Diameter and Simple Tool to Evaluate Their Diameter, Concentration and Yield. Chemistry Select 2019, 4, 2716-2720.
- (61) Sun, Y.; Gates, B.; Mayers, B.; Xia, Y. Crystalline Silver Nanowires by Soft Solution Processing. Nano Lett. 2002, 2, 165-168. (62) Yoshikawa, H.; Hieda, K.; Ikeda, K.; Tamiya, E. Hydrogen Peroxide Detection with a Silver Nanoparticle Grating Chip Fabricated by Plasmonic Plating. Anal. Methods 2019, 11, 2991-2995. DISSONAHAMAG PHONFORLEY, AG MINOVZANBUNOPOWATH HEREN ALIMERN & C. for Both Tailoring the Optical Properties and Measuring the H2o2 Concentration. J. Phys. Chem. C 2010, 114, 6396-6400.
- (64) Zhai, W.; Sun, F.; Chen, W.; Pan, Z.; Zhang, L.; Li, S.; Feng, S.; Liao, Y.; Li, W. Photodegradation of P-Nitrophenol Using Octahedral Cu2o Particles Immobilized on a Solid Support under a Tungsten Halogen Lamp. Appl. Catal. A: Gen 2013, 454, 59-65.
- (65) Wang, X.; Huang, S.; Zhu, L.; Tian, X.; Li, S.; Tang, H. Correlation between the Adsorption Ability and Reduction Degree of

Graphene Oxide and Tuning of Adsorption of Phenolic Compounds. Carbon 2014, 69, 101-112.

(66) Jiu, J.; Araki, T.; Wang, J.; Nogi, M.; Sugahara, T.; Nagao, S.; Koga, H.; Suganuma, K.; Nakazawa, E.; Hara, M.; Uchida, H.; Shinozaki, K. Facile Synthesis of Very-Long Silver Nanowires for Transparent Electrodes. J. Mater. Chem. A 2014, 2, 6326-6330.

(67) Wei, Z.; Liu, C.-H.; Duan, H.; Luo, Q.; Huang, M.; Thanneeru, S.; Nieh, M.-P.; He, J. Self-Assembly of Gold Nanoparticles Grafted with Amphiphilic Supramolecular Block Copolymers. Giant 2022, 10, 100102.

□ Recommended by ACS

Smart Anisotropic Colloidal Composites: A Suitable Platform for Modifying the Phase Transition of Diblock Copolymers by Gold Nanoparticles

Ritu Yadav, Pannuru Venkatesu, et al.

MARCH 21, 2023

LANGMUIR

READ 🗹

Uniform Gold Nanoclusters Supported on Mesoporous Polymer Beads Decorated with Polyaminophosphine Patches for the Catalytic Reduction of 4-Nitrophenol

Xiaoqiu Yao, Decheng Wan, et al.

MARCH 20, 2023

ACS APPLIED NANO MATERIALS

RFAD 🗹

Poly(N-heterocyclic carbene)-Protected Water-Soluble Gold **Nanoparticles with Tunable Functions for Biosensing Applications**

Xiujuan Qiao, Ying-Feng Han, et al.

JANUARY 23, 2023

ACS APPLIED NANO MATERIALS

READ **C**

Electronic Tuning of Gold Nanoparticle Active Sites for Reduction Catalysis

Sayed Abu Sufyan, Michael M. Nigra, et al.

DECEMBER 29, 2022

ACS APPLIED MATERIALS & INTERFACES

READ 🗹

Get More Suggestions >